Materials Research Bulletin 162 (2023) 112193

Contents lists available at ScienceDirect

Materials Research Bulletin

journal homepage: www.elsevier.com/locate/matresbu

Research Papers

Energetically preferred Li^+ ion jump processes in crystalline solids: Site-specific hopping in β-Li_3VF_6 as revealed by high-resolution ^6Li 2D EXSY NMR

Patrick Bottke [a,b], Katharina Hogrefe [a], Julia Kohl [c], Suliman Nakhal [c], Alexandra Wilkening [a], Paul Heitjans [d], Martin Lerch [c], H. Martin R . Wilkening [a,e,*]

[a] Graz University of Technology, Institute of Chemistry and Technology of Materials, (NAWI Graz), Stremayrgasse 9, 8010 Graz, Austria
[b] Carl von Ossietzky University Oldenburg, Institute of Chemistry, Carl-von-Ossietzky Str. 9-11, 26129 Oldenburg, Germany
[c] Technische Universität Berlin, Fakultät II, Institut für Chemie, Straße des 17. Juni 135, 10623 Berlin, Germany
[d] Leibniz Universität Hannover, Institut für Physikalische Chemie und Elektrochemie, Callinstraße 3-3a, 30167 Hannover, Germany
[e] Christian Doppler Laboratory for Lithium Batteries, Stremayrgasse 9, 8010 Graz, Austria

ARTICLE INFO

Keywords:
NMR
Self-diffusion
Cathode materials
Exchange processes

ABSTRACT

The visualization of atomic or ionic jump processes on the Ångström length scale is important to identify the preferred diffusion pathways in solid electrolytes for energy storage devices. Two-dimensional high-resolution ^6Li nuclear magnetic resonance (NMR) spectroscopy is highly suited to yield unprecedented site-specific insights into local Li^+ exchange processes within a single measurement. Here, the beta-modification of Li_3VF_6 is used as a model system for such an investigation as it provides a range of important Li^+ geometric environments in one and the same crystal structure useful to elucidate qualitatively a ranking of energetic preferences of the Li^+ exchange processes. In Li_3VF_6 the Li^+ ions are subject to diffusive exchange processes among five crystallographically and magnetically inequivalent Li sites: LiF_n (n = 6, 4). By using a sample with a natural concentration of the ^6Li isotope, we suppressed unwanted spin-diffusion processes and visualized the various exchange processes on the ms time scale. We were able to verify the following ranking experimentally: Li^+ ion jumps between face-shared polyhedra are preferred, followed by Li^+ exchange between edge-shared configurations for which interstitial sites are needed to jump from site to site. Surprisingly, Li^+ exchange between corner-shared polyhedra and Li^+ hopping involving almost isolated LiF_4 polyhedra do contribute to overall Li^+ self-diffusion as well. In this sense, the current study experimentally verifies current predictions by theory but also extends our understanding of ion dynamics between corner-shared Li-bearing polyhedra.

1. Introduction

The site-specific characterization of Li^+ jump processes in solids increasingly gains in importance to understand the conduction mechanisms of ceramic electrolytes and active materials for lithium-based batteries [1–6]. Probing the energetic preferences of the mobile ions while diffusing through a given crystal lattice with suitable experiments will help us verifying atomic-scale predictions from theory [3,4,7]. Such knowledge is ultimately needed to identify the most suitable electrolytes and to set up the right design rules [3,4,8] to prepare active materials with tailored diffusion properties.

For this purpose, we have chosen a cathode material, namely beta-Li_3VF_6 [9], that comprises several important LiF_n (n = 4, 6) polyhedra connections useful to establish a ranking of the energetically favored jump processes. In the beta-modification of Li_3VF_6 (crystallizing with C2/c symmetry, beta-Li_3AlF_6-type, see Fig. 1) the Li^+ ions occupy five crystallographically and magnetically inequivalent sites. It serves as an excellent model system as it provides all important Li^+ geometric environments in one and the same crystal structure. Jumping of the ions among these sites, and in the presence of an external magnetic field, is probed by taking advantage of the hyperfine (Fermi contact) interactions of the magnetic moments of the $^6Li^+$ nuclei (spin-quantum number I = 1) with local magnetic fields in the monoclinic vanadium fluoride. ^6Li MAS NMR, see refs. [10,11] for a general overview, has

* corresponding author.
E-mail address: wilkening@tugraz.at (H.M.R. Wilkening).

https://doi.org/10.1016/j.materresbull.2023.112193
Received 28 October 2022; Received in revised form 7 February 2023; Accepted 9 February 2023
Available online 16 February 2023

extensively been used by Grey and co-workers as well as by Delmas and co-workers to study local environments of Li ions in paramagnetic cathode materials [12–20]. These earlier studies, see, e.g., refs. [14,18, 20,21], in particular, do also entail detailed information about the basics behind 2D NMR and hyperfine interactions.

Here, we used a sample with natural ^{6}Li abundance (7.5%). In this sample, ^{6}Li dilution eliminates interfering ^{6}Li-^{6}Li spin-diffusion effects and, thus, gives access to undisturbed 2D high-resolution ^{6}Li exchange nuclear magnetic resonance (NMR) spectra [17,21-32]. In the same way, one could have used a ^{7}Li diluted sample, see, e.g., similar studies by Kroeker et al. [33]. These ^{6}Li 2D NMR spectra, together with the corresponding 1D NMR data, provided direct insights into the relevant jump mechanisms. In agreement with predictions from theory [3], Li^+ jumps between face-shared geometries are energetically favored against those between edge-shared polyhedra involving temporarily occupied tetrahedral interstitial sites. Li^+ ions located in tetrahedral polyhedra do take part in overall self-diffusion to a much lesser extent.

2. Experimental

The polycrystalline Li_3VF_6 sample was prepared by a sol-gel route involving annealing steps at high temperatures (600 °C). Slow cooling to room temperature resulted in the phase pure monoclinic phase of Li_3VF_6; details on sample preparation, the precursors used and characterization by means of X-ray powder diffraction are given elsewhere [34].

To record ^{6}Li and ^{7}Li NMR spectra the powder sample was packed in 1.3-mm rotors. Spectra were recorded with a Bruker MAS probe and an Avance III spectrometer operating at 14.1 T yielding resonance frequencies of 88 MHz (^{6}Li) and 233 MHz (^{7}Li). LiCl (aq, 1 M; 0 ppm) served as reference to determine NMR chemical shifts. The rotor spinning speed was 60 kHz, pulse lengths ranged from 2 to 2.5 μs slightly depending on temperature. While 1D NMR spectra were acquired with a single 90° pulse sequence, we used the well-known NOESY (nuclear Overhauser and exchange spectroscopy) pulse sequence to record 2D spectra at different mixing times, see also ref. [24]. 1D spectra were recorded at temperatures ranging from 289 K to 400 K, while 2D exchange spectra have solely been recorded at 338 K. The temperature was adjusted with heated bearing gas and type-T thermocouples near the rotor. Rotation synchronized acquisition was performed in both F2 and F1 directions; states-TPPI (time-proportional phase incrementation) for quadrature detection in F1 and phase correction in F1 direction were employed. The recycle delay between each scan was at least $5T_1$ with T_1 being the corresponding Li NMR spin-lattice relaxation time. The rates $1/T_1$ were determined using the inversion recovery pulse sequence [35].

3. Results

Fig. 1 shows the monoclinic crystal structure of Li_3VF_6 with its five magnetically (and crystallogrpahically) inequivalent Li sites Li1, Li2, Li3, Li4, and Li5 [34]. Li2 is tetrahedrally coordinated by four F anions; the other Li ions reside in slightly distorted octahedral voids $LiF_{n=6}$. The 5 individual sites are fully occupied by Li^+. According to the number of the available sites, we expect that the area under the NMR signal for Li1 (Wyckoff position 4e) is half of that of any of the other lines for which we expect the same area (or intensity). Indeed, the 1D ^{6}Li MAS NMR spectrum recorded at room temperature (see Fig. 2) reveals an area ratio of ca. 0.5:1:1:1:1 as expected from the number of available Li sites. Hence, we can already conclude that the signal (E) shifted downfield strongest and appearing at 83(2) ppm reflects the Li1 site. This site shares a common edge with the Li4 octahedron and, thus, we expect facile exchange processes between Li1 and Li4 through the temporary occupation of the tetrahedral void connection the two polyhedra by face sharing, see Fig. 1a.

Considering the five distinct lines in ^{6}Li NMR, we see that they shift linearly with the inverse temperature $1/T$ towards higher ppm values, see the inset in Fig. 2b. This upfield shift is ascribed to Curie-Weiss behavior [36] of the bulk magnetic susceptibility being affected by thermal fluctuations of the spin moments. The largest shift is seen for signal E, that is, for the Li site, reflecting the nucleus subjected to the largest hyperfine interaction. We assume that Curie-Weiss susceptibility dominates these ^{6}Li NMR shifts over other contributions such as van Vleck susceptibility and/or Pauli paramagnetism for which temperature independent NMR lines are expected. The same holds for the effect of any diamagnetic susceptibilities on the NMR lines.

In order to assign also the remaining four NMR lines to the available crystallographic Li positions, we qualitatively estimated the extent of electron spin density transfer from the octahedral V^{3+} centers (with two unpaired electrons) to the octahedrally coordinated Li nuclei [12,14,18, 20,26]. Thus, the following analysis does not include the tetrahedral Li2 site; this site is discussed separately (see below). In the case of Li_3VF_6, we deal with a $t_{2g}^2e_g^0$ configuration of the octahedral crystal field splitting,

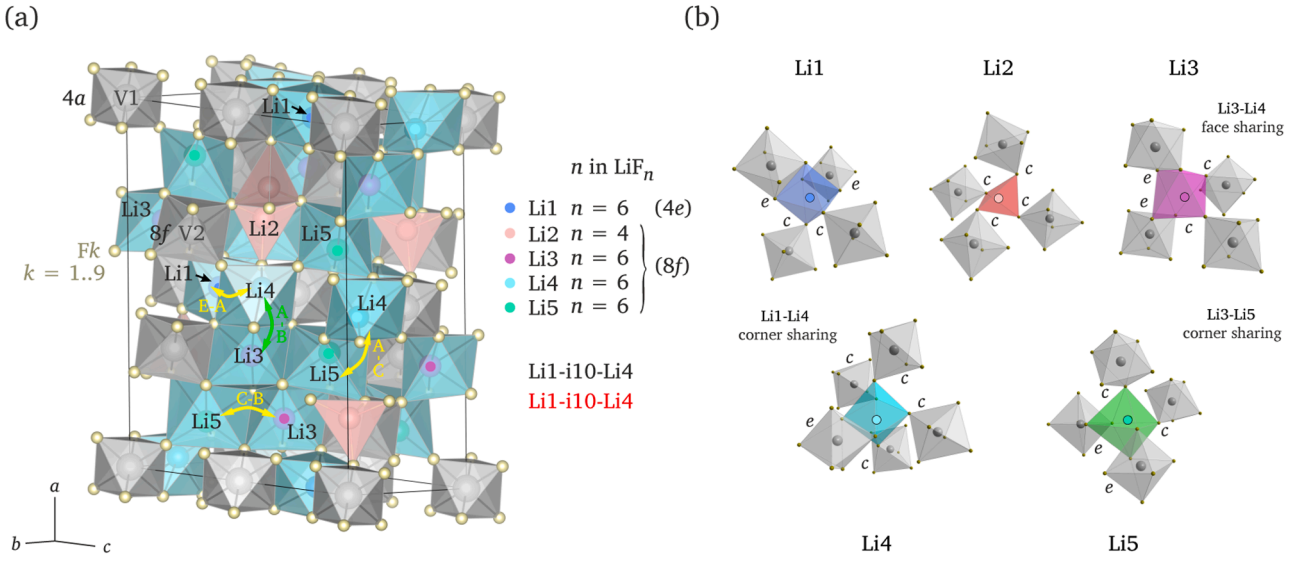

Fig. 1. (a) Crystal structure of monoclinic Li_3VF_6 with the five distinct Li ions highlighted. V occupies the positions V1(4*a*) and V2(8*f*). Altogether the structure is composed of nine different F anions F*k*, with $k = 1..9$. Arrows indicate the jump processes as seen by 2D ^{6}Li NMR. (b) The individual Li sites and their connections (c: corner sharing, e: edge sharing) to the neighboring VF_6 octahedra.

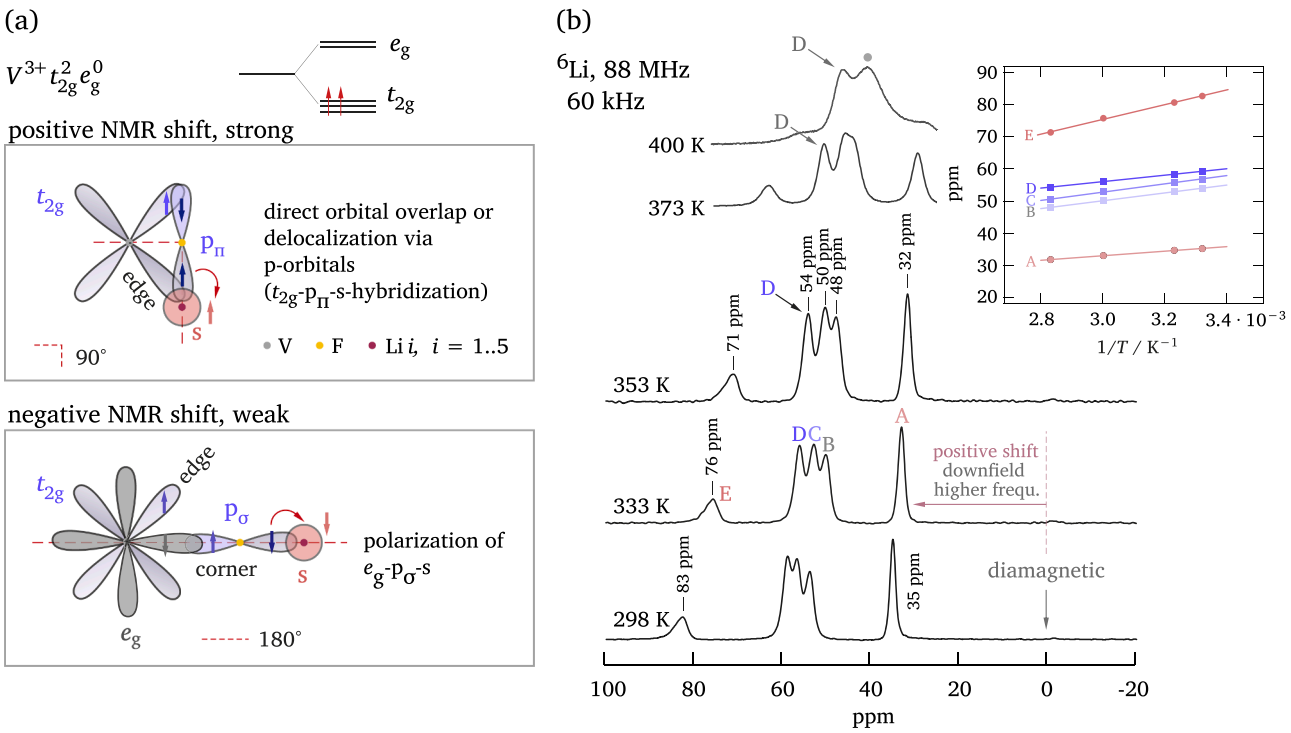

Fig. 2. (a) The relevant mechanisms of positive (delocalization) and negative (polarization) spin density transfer for octahedrally coordinated V^{3+} with $t_{2g}^2e_g^0$ configuration. (b) ^{6}Li MAS NMR spectra of Li_3VF_6 recorded at 60 kHz spinning speed and at the temperatures indicated. Hardly no diamagnetic impurity is seen around 0 ppm. Note that the spectra recorded at 373 K and 400 K were acquired at a spinning speed of only 15 kHz. Effectively all signals are shifted downfield because of Fermi contact hyperfine interactions through the transfer of positive spin density from V^{3+}. The Curie-Weiss temperature behavior of the NMR positions on the ppm scale is shown in the inset. At $T > 373$ K a coalesced line emerges, which is marked by a circle. This coalescence effect leads to a significant reduction of the signals E and A.

which gives rise to the two transfer mechanisms [24,26] depicted in Fig. 2a. It is either possible to transfer spin density via the delocalization mechanism (upper illustration) or the polarization mechanism (illustration at the bottom). In the case of the rather strong delocalization mechanism, positive spin density is either transferred directly or via effective orbital overlap involving the p-orbitals of the F anions. The latter requires a V-F-Li angle of 90°. If this geometric configuration is fulfilled, we expect the corresponding ^{6}Li and ^{7}Li NMR signals to be shifted toward positive ppm values. An opposite, but weaker, shift is possible via the 180° orbital interaction, polarizing the orbitals linearly connecting the three atoms. Hence, a proper assignment might be possible by taking into account bond distances, considering the number of V centers in the direct neighborhood of the Li nuclei and by analyzing the V-F-Li bond angles for the five Li sites in Li_3VF_6.

Our geometric analysis, using the Li environments shown in Fig. 1b, resulted in the following assignment. Starting with Li1 in $Li1F_6$ we notice that this octahedron is connected to two VF_6 polyhedra by edge sharing (e) and to two other VF_6 octahedra by corner sharing (c). According to the delocalization mechanism, we have four Li-V-F angles that are close to 90°; two of them amount to 96°. The corresponding angles with the edge-sharing $VF_{n=6}$ polyhedra strongly deviate from 180° and amount to ca. 130°. These angles are listed in Table 1 for all Li sites. Disregarding the assignment of Li1 already given above for a while, solely the fact that four 90° angles determine the Fermi-contact interactions of Li1 leads us to the assumption that this Li spin produces an NMR signal with a large positive shift on the ppm scale. Therefore, it is either responsible for the NMR line labeled D or for the line labeled E in Fig. 2b. This assignment is based merely on the fact that the other LiF_n polyhedra are characterized by not more than one or two of such beneficial configurations with angles ranging from 92° to ca. 95°, see Table 1. It fully agrees with the structural considerations mentioned above, which already identified Li1 to reflect the NMR signal

Table 1
Li-F-V angles characterizing the geometric connection of the Li octahedral sites with the $VF_{n=6}$ polyhedra. (e) denotes connection via common edges and (c) means that the two polyhedra are connected by sharing common corners. Angles written in bold are close to 90° being the optimal angle to enable effective transfer of positive spin density via the delocalization mechanism. No angles close to 180° describe the situation in monoclinic Li_3VF_6.

Li site	Li-F-V angle / °					
Li1 (E)	Li1-F6-V1(e)-F9-Li1		Li1-F6-V1(e)-F9-Li1		F1-V2(c)	F1-V2(c)
Li1-F-V	**98.200**	**96.287**	**98.200**	**96.287**	129.591	129.591
Li2	F6-V1(c)	F4-V2(c)	F8-V2(c)	F8-V2(c)	-	-
Li2-F-V	118.983	124.695	125.208	129.151		
Li3	F5-V1(c)	F2-V2(c)	Li3-F1-V2(e)-F4-Li3		Li3-F2-V2(e)-F7-Li3	
Li3-F-V	126.928	160.704	103.605	**92.079**	106.394	**93.488**
Li4 (A)	Li4-F5-V1(e)-F6-Li4		F1-V2(c)	F3-V2(c)	F7-V2(c)	F7-V2(c)
Li4-F-V	**94.845**	100.028	131.914	129.776	130.270	134.135
Li5	F5-V1(c)	F9-V1(c)	Li5-F2-V2(e)-F3-Li5		Li5-F4-V2(e)-F8-Li5	
Li5-F-V	124.306	133.026	**92.174**	104.751	110.04	**92.565**

E. In excellent agreement with the results in Fig. 2b (see inset), the NMR line shift of signal E shows the strongest dependence on temperature.

Li2 takes a special position as it is coordinated not by six but only by four F anions. In such a case, positive spin density could be transferred from the VF_6 center via a V-F-Li geometry that is characterized by an angle of slightly more than 120°. One might assume transfer of electron spin density from the t_{2g} orbital via the p orbitals of F according to a delocalization mechanism. Carlier et al. [18] described such a mechanism for electron spins in the e_g orbital rather than in t_{2g} transferring positive polarization to Li in a tetrahedral coordination. We think that the Li2-F-V angles of Table 1, turning out to be slightly larger than 120°, do indeed lead to a noticeable transfer of positive spin density. We assume, however, this transfer to be weaker than that governing the shift of the Li1 line (see above). Hence, also Li^+ on the Li2 sites should

produce an NMR line shifted toward relatively large ppm values. However, considering the rather strong polarization transfer through the four 90° interactions characterizing $Li1F_{n=6}$ and the fact that there are less Li1 ions than Li2 ions in one formula unit Li_3VF_6, the NMR signal E, with the lowest intensity, is undoubtedly assigned to Li1. Li2 seems to give rise, on the other hand, to signal D, as will be explained below.

From the remaining LiF_n polyhedra ($Li3F_6$, $Li4F_6$, $Li5F_6$), the one of Li4 has only a single geometric possibility to receive positive spin polarization, see the Li4-F-V angle of ca. 95° in Table 1. This situation is in contrast to the geometries of Li3 and Li5 sharing common edges with two VF_6 units. The Li site Li4 is, therefore, assigned to the NMR line with the weakest shift appearing at 35(2) ppm and labeled A in Fig. 2b. For Li3 and Li5, the assignment, solely using bond angles and transfer mechanisms, remains, however, unclear so far.

Hence, to present a complete assignment, we carried out 2D ^{7}Li and ^{6}Li MAS NMR to visualize which Li sites are able to exchange Li^+ ions. The corresponding contour ^{7}Li and ^{6}Li NMR plots recorded at varying mixing times are shown in Fig. 3 and Fig. 4. Attempts to use the ^{7}Li nucleus for this purpose failed as the strong dipolar interactions in a sample with natural ^{7}Li abundance yield off-diagonal intensities that reflect spin-diffusion rather than particle diffusion. These intensities are seen in the contour plots of Fig. 3; the 2D spectra were recorded at mixing times of 3 ms and 12 ms, respectively. Even at a rather short mixing time of only 3 ms we cannot suppress the detrimental influence of (spectral) spin diffusion in frequency space [37].

Fortunately, switching to the spatially diluted ^{6}Li nucleus [33], possessing a by a factor of 1/50 lower quadrupole moment and exposed too much weaker dipole-dipole interactions, the picture completely changes. In ^{6}Li NMR, spin diffusion artifacts, which mainly affected the three closely spaced NMR lines around 55 ppm, fully disappeared at 12 ms (see Fig. 4). This circumstance enabled us to study the Li^+ ion exchange processes in detail, free of any detrimental influences.

At short mixing times, we see a pronounced Li exchange process that involves the lines A and B (Fig. 4a). Line A has been assigned to Li4, whose F anion polyhedron shares a common face with the $Li3F_6$ polyhedra. Here, we remember that Li4 and Li3 are the only Li sites that are connected by face sharing; the interatomic distance is only 2.8 Å. Therefore, the most prominent exchange process seen in 2D ^{6}Li MAS NMR is ascribed to jumping of Li^+ between these two positions which leads us to the conclusion that line B represents Li^+ on Li3.

The second exchange process concerns the signals E and A. With the sites assigned above, the corresponding off-diagonal intensities mirror Li1-Li4 exchange processes. Indeed, the polyhedra $Li1F_6$ and $Li4F_6$ are neighbors connected by sharing a joint edge. The tetrahedral void between the two polyhedra is used as a transition site (i10) to jump from Li1 to Li4 (distance ca. 3.1 Å) and *vice versa*.

Knowing that Li3 is reflected by line B, we ascribe the B-C exchange process seen to hopping processes between $Li3F_6$ and $Li5F_6$ connected to each other by sharing common edges with i5 being the tetrahedral void in between. Hence, signal C reflects the Li5 ions.

The cross peaks connecting the lines A (Li4) and C (Li5) reflect another prominent exchange process. Although the $Li4F_6$ polyhedron does not share a joint edge with $Li5F_6$, there is relatively large interstitial space (see i1 in Fig. 5a) connecting these two polyhedra. Note that in another configuration the distance between Li3 and Li5 is only 3.3 Å which also allows for appreciable exchange processes via interstitial space. Li4-Li5 exchange is possible involving essentially two pathways viz. using the interstitial sites i1, i3 and i7, see also Fig. 5.

Although there is no edge-sharing connection between $Li2F_4$ and $Li5F_6$, the arrangement of the two almost isolated $Li2F_4$ tetrahedra suggests to some extent Li5-Li2 exchange processes. Additional pathways involving Li2 are indicated in Fig. 5 as well and will be discussed below. Assigning Li2 to signal D would be not in contradiction to the estimations from the bond angle analysis discussed above. NMR tells us that any further exchange processes, particularly those involving Li2, seem to be energetically less favored in Li_3VF_6. This statement is further corroborated by considering the ^{6}Li MAS NMR spectra recorded at 373 K and 400 K, as presented in Fig. 2b. They reveal that line D (Li2) is hindered in contributing to a coalesced signal that emerges at temperatures higher than 373 K. This coalesced signal, marked in Fig. 2b with a circle, is best seen at 400 K. It is mainly involving the lines A and E (most likely also B), as is fully in line with ^{6}Li 2D NMR (see Fig. 4b).

To prove the above-mentioned assignment further, we looked at all connectivities of the polyhedra, either via face, edge or corner sharing, and the number of Li neighbors, see Table 2. We infer from Table 2 that apart from the direct Li^+ exchange via face sharing of $Li3F_6$ and $Li4F_6$ (see the last column), $Li3F_6$ is connected to two $Li5F_6$ polyhedra by sharing common edges and to another $Li3F_6$ polyhedra by sharing a joint edge. The latter would give rise to a broadening of the diagonal NMR intensities, which is, however, hardly seen in our NMR plots. For one of the two tetrahedral sites, connecting one $Li3F_6$ octahedral with another $Li5F_6$ octahedral by face sharing, we expect Li^+-V^{3+} repulsive interactions if Li^+ temporarily occupies the tetrahedral void reducing the probability of Li5-Li3 exchange somewhat. Only for the second pathway, no such interaction is expected. Altogether, repulsive Li^+-V^{3+} interactions might serve as an argument for the rather weak B-C cross peaks in Fig. 4b. For the geometrically similar configuration Li1-Li4, no such direct repulsion is expected.

In summary, considering especially Table 2, jumps between Li3 and Li4 as well as between Li4 and Li1 enable the Li ions to move over long distances taking, most likely, also advantage from exchange processes between Li3 and Li5. The Li1-$(Li4\text{-}Li3)_{face}$-Li5 pathway leads to 3D Li^+

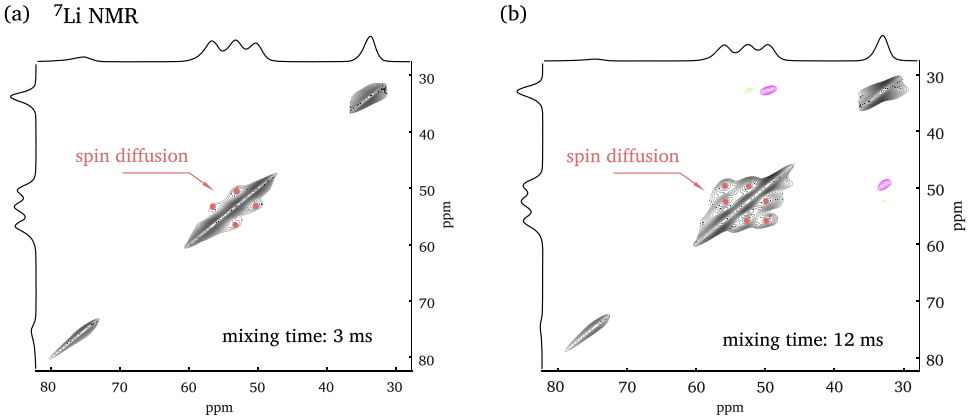

Fig. 3. 2D ^{7}Li ($I = 3/2$) MAS NMR spectra (233 MHz, 338 K) of Li_3VF_6 recorded at mixing times of 3 ms (a) and 12 ms (b), respectively. Off-diagonal intensities represent artifacts, most likely because of dipolarly coupled ^{7}Li spins leading to spectral spin diffusion. These cross-peaks signals are not caused by particle self-diffusion.

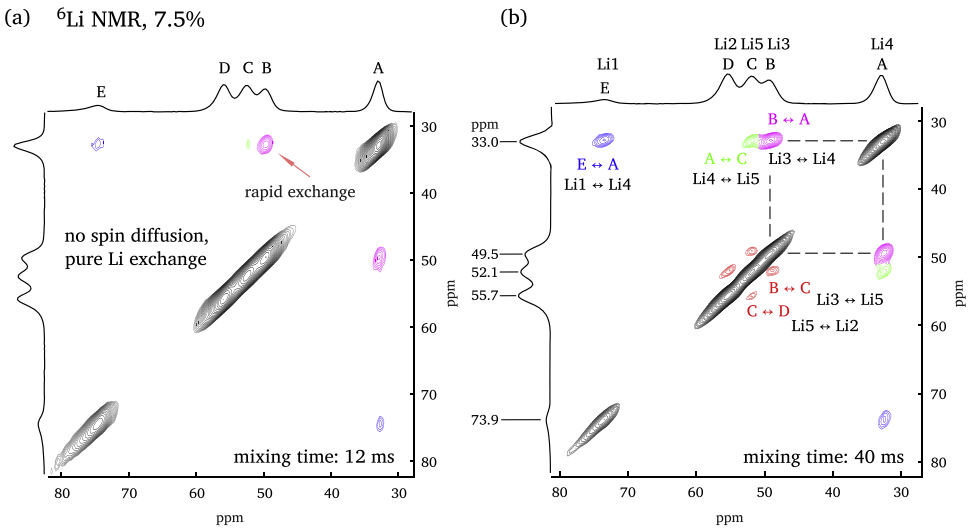

Fig. 4. 2D ^{6}Li ($I = 1$) MAS NMR spectra (88 MHz, 338 K) of Li_3VF_6 recorded at mixing times of 12 ms (a) and 40 ms (b), respectively. The cross peaks connecting the lines A and B reveal facile Li^+ hopping between the sites Li4 and Li3 whose octahedra are connected by sharing common faces. Exchange processes between Li4 and Li1 as well as between Li4 and Li5 involve suitable interstitial sites enabling Li^+ hopping. As an example, Li1-Li4 and Li3-Li5 hopping processes involve the tetrahedral interstitial voids i10 and i5 (see Fig. 1 and Fig. 5), respectively.

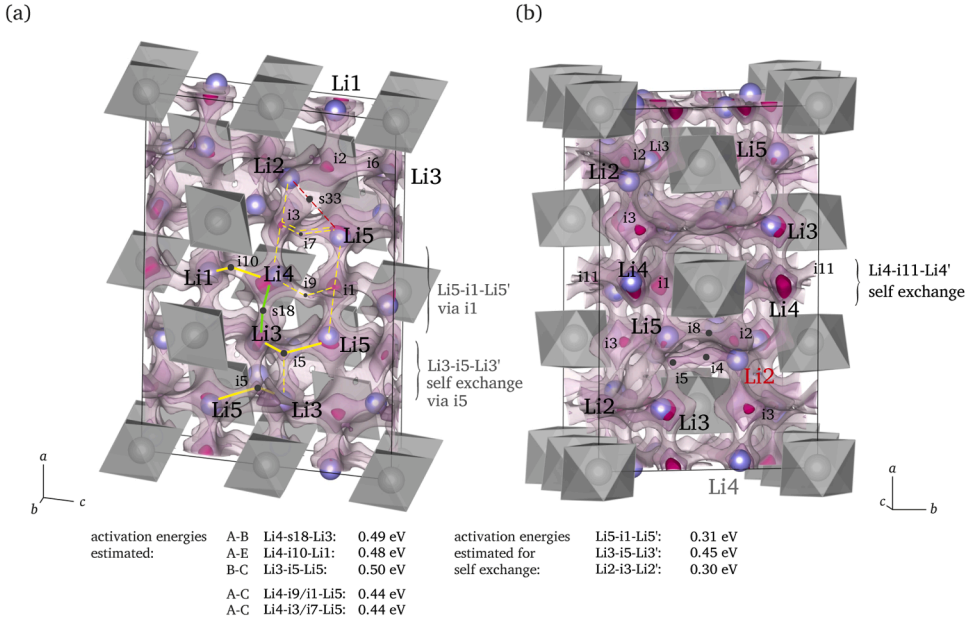

Fig. 5. (a) Estimated results of our softBV analysis highlighting the interstitial voids connecting the regularly occupied Li sites in monoclinic Li_3VF_6. Selected pathways are drawn with solid and dashed lines. Li3-Li4 exchange proceeds via the saddle point s18; most of the activation energies are centered around 0.5 eV. (b) Li2 in tetrahedral F anion coordination has access to other Li sites via i3, i2, (i3-i7), (i4-i5), and (i2-i6) able to reach all the other positions incl. Li2' (via i3). In 2D NMR, we are only able to verify exchange between Li2 and Li5, which, most likely, proceeds via (i3-i7, 0.31 eV). Direct jumps Li2-Li5 are to be characterized by a rather high activation energy of ca. 0.69 eV, see (a).

transport on a macroscopic length scale. Moreover, NMR suggests that the Li5 ions exchange with those on Li4 via relatively large empty interstitial voids.

Altogether, this picture is in the most important aspects underpinned by our softBV analysis [38–40], see Fig. 5, which alternatively does also point to further diffusion pathways. Apart from Li3-Li4 exchange via s18, and hopping between Li4 and Li1 via i10, we also recognize the Li3-Li5 exchange process using the interstitial site i5.

As suggested by the isosurfaces drawn in Fig. 5, jumping between Li4 and Li5 is possible via two-step diffusion processes using the pathways Li4-i3-i7-Li5 and Li4-i9-i11-Li5 suggesting indeed the involvement of larger interstitial voids as discussed above. Self-exchange processes are formally possible for Li4 (via i11), Li5 (via i1) and even for Li2 (via i3).

The involvement of Li2 in overall Li^+ hopping in Li_3VF_6 is also highlighted in Fig. 5a and Fig. 5b. Several possibilities are suggested, such as hopping from Li2 to Li4 or Li1 using the interstitials i3 (Fig. 5b) and i2 (Fig. 5a). Jumping from Li2 to Li3 requires two steps: Li2-i2-i6-Li3. In NMR, we cannot find any strong evidence for such processes for which the softBV analysis yields activation energies ranging from 0.3 to 0.46 eV. The pathway Li2-i3-Li4, see Fig. 5b, would suggest to identify line C in Fig. 4b with Li2 rather than with Li5. Changing the assignment of Li2 and Li5 would, however, mean that no Li3-Li5 exchange would take place, as there is no D-B cross peak visible in 2D NMR. Such a process is, however, likely, as the polyhedra $Li5F_6$ and $Li3F_6$ are connected by sharing common edges, as discussed above, see also Table 2. Hence, we tend to leave the assignment presented in Fig. 5b as it is, that is, suggesting two two-step Li4-Li5 (A-C) and Li2-Li5 (C-D) exchange processes taking place in Li_3VF_6.

Estimated activation energies characterizing the hopping processes revealed in 2D NMR are included in Fig. 5 as well. We notice that they range from approximately 0.45 to 0.5 eV, hence they turn out to be higher than those obtained by *ab initio* molecular dynamics studies for Li_3MF_6, M = Al, Ga, Sc (0.23 to 0.33 eV) [9]. Activation energies ranging from approximately 0.2 to 0.35 eV have also been found for the alpha modification of Li_3VF_6 by first principle calculations [41]. Such activation energies indirectly point to jump rates in the lower kHz range to which 2D NMR with mixing times of up to 40 ms would be sensitive, as it has been shown for the alpha modification of Li_3VF_6 earlier [24].

Table 2
Li sites and the number of Li neighbors in monoclinic Li_3VF_6. The second is to read as follows: Li1 has eight different Li neighbors in its first coordination shell, these are the Li ions Li2, Li3, Li4 and Li5. The superscript number tells us how many of, *e.g.*, Li1 ions are in the direct vicinity of Li1: 3^2 means two Li3 neighbors. The same notation is used to count the polyhedra to which each LiV_n polyhedron is connected.

Li site	no. and kind of Li neighbors	corner	edge	face
Li1 or $Li1V_6$	8 $2^2\ 3^2\ 4^2\ 5^2$	6 $2^2\ 3^2\ 5^2$	2 4^2 (E-A)	- -
Li2 or $Li2V_4$	7 $1^1\ 2^1\ 3^1\ 4^2\ 5^2$	6 $1^1\ 3^1\ 4^1\ 5^3$ (D-C)	1 2^1	- -
Li3 or $Li3V_6$	7 $1^1\ 2^1\ 3^1\ 4^2\ 5^2$	3 $1^1\ 2^1\ 4^1$	3 $3^1\ 5^2$ (B-C)	1 4^1 (B-A)
Li4 or $Li4V_6$	7 $1^1\ 2^1\ 3^2\ 4^1\ 5^2$	4 $2^1\ 3^1\ 5^2$ (A-C)	2 1^1 (E-A) 4^1	1 3^1 (B-A)
Li5 or $Li5V_6$	8 $1^1\ 2^3\ 3^2\ 4^2$	6 $1^1\ 2^3\ 4^2$	2 3^2 (B-C)	- -

4. Conclusion

Taken together, the five Li NMR lines, clearly resolved in a (1D) ^{6}Li NMR experiment, have fully been assigned to the regularly occupied Li sites in monoclinic Li_3VF_6. Our assignment suggested solely grounds on crystallographic information and a single set of mixing-time dependent 2D ^{6}Li MAS NMR spectra. Our study unequivocally identifies the sites (Li4, Li3, Li1) preferentially involved in Li diffusion, hence shedding light on the most probable diffusion pathways in Li_3VF_6. We demonstrate that hopping between polyhedra connected by common faces (Li3-Li4) is energetically favored against hopping processes using interstitial voids acting as transition states. In this sense, it is a direct experimental verification of recent predictions by theory.

Surprisingly, our study shows that we should not underestimate jump processes between corner sharing polyhedra. In Li_3VF_6, our soft BV analysis revealed rather suitable Li interstitial voids (e.g., i1) that connect these Li sites (Li4-Li5) leading to the measurable off-diagonal intensities in ^{6}Li 2D exchange NMR. However, as is rather conscientiously shown by NMR, the Li^+ ions on the tetrahedral position Li2 do take part in overall Li^+ diffusion to a much lesser extent than the other Li ions. Despite the fact that the Li2 ions have access to rather large interstitial sites connecting Li2 with, e.g., Li5 and Li3, the NMR experiments tell us that Li^+ seems to be less mobile if starting from the tetrahedrally coordinated Li2 position.

In summary, in Li_3VF_6 we clearly see rapid exchange between face-sharing Li octahedra, followed by (i) translational processes between edge-sharing octahedra and (ii) hopping between corner-shared octahedra via suitable interstitial sites. Li^+ in tetrahedral configuration is energetically, however, less favored, even if (or because) we (must) consider large interstitial voids connecting the polyhedra.

CRediT authorship contribution statement

Patrick Bottke: Investigation, Methodology, Formal analysis, Visualization, Writing – review & editing. **Katharina Hogrefe:** Investigation, Formal analysis, Visualization. **Julia Kohl:** Investigation, Formal analysis. **Suliman Nakhal:** Investigation, Formal analysis. **Alexandra Wilkening:** Investigation, Formal analysis, Visualization. **Paul Heitjans:** Conceptualization, Formal analysis, Writing – review & editing. **Martin Lerch:** Conceptualization, Formal analysis, Writing – review & editing. **H. Martin R . Wilkening:** Conceptualization, Methodology, Formal analysis, Visualization, Writing – original draft, Writing – review & editing, Supervision, Funding acquisition.

Declaration of Competing Interest

The authors declare that they have no known competing financial interests or personal relationships that could have appeared to influence the work reported in this paper.

Data availability

Data will be made available on request.

Acknowledgements

We thank the former DFG Research Unit 1277 for financial support. Moreover, financial support by the comet project safeLIB of the FFG (Austrian Research Promotion Agency) is highly acknowledged.

References

[1] Y. Gao, A.M. Nolan, P. Du, Y. Wu, C. Yang, Q. Chen, Y. Mo, S.-H. Bo, Classical and Emerging Characterization Techniques for Investigation of Ion Transport Mechanisms in Crystalline Fast Ionic Conductors, Chem. Rev. 120 (2020) 5954–6008.
[2] A.M. Nolan, Y. Zhu, X. He, Q. Bai, Y. Mo, Computation-Accelerated Design of Materials and Interfaces for All-Solid-State Lithium-Ion Batteries, Joule 2 (2018) 2016–2046.
[3] X.F. He, Y.Z. Zhu, Y.F. Mo, Origin of Fast Ion Diffusion in Superionic Conductors, Nat. Commun. 8 (2017) 15893 (15891)-15893(15897).
[4] Y. Wang, W.D. Richards, S.P. Ong, L.J. Miara, J.C. Kim, Y.F. Mo, G. Ceder, Design Principles for Solid-State Lithium Superionic Conductors, Nat. Mater. 14 (2015) 1026–1031.
[5] B.J. Morgan, Mechanistic Origin of Superionic Lithium Diffusion in Anion-Disordered Li_6PS_5X Argyrodites, Chem. Mater. 33 (2021) 2004–2018.
[6] J.C. Bachman, S. Muy, A. Grimaud, H.H. Chang, N. Pour, S.F. Lux, O. Paschos, F. Maglia, S. Lupart, P. Lamp, L. Giordano, Y. Shao-Horn, Inorganic Solid-State Electrolytes for Lithium Batteries: Mechanisms and Properties Governing Ion Conduction, Chem. Rev. 116 (2016) 140–162.
[7] K. Jun, Y. Sun, Y. Xiao, Y. Zeng, R. Kim, H. Kim, L.J. Miara, D. Im, Y. Wang, G. Ceder, Lithium Superionic Conductors with Corner-Sharing Frameworks, Nat. Mater. 21 (2022) 924–931.
[8] S. Ohno, A. Banik, G.F. Dewald, M.A. Kraft, T. Krauskopf, N. Minafra, P. Till, M. Weiss, W.G. Zeier, Materials Design of Ionic Conductors for Solid State Batteries, Progr. Energy 2 (2020), 022001.
[9] B. Zhang, J. Zhong, Y. Zhang, L. Yang, J. Yang, S. Li, L.-W. Wang, F. Pan, Z. Lin, Discovering a New Class of Fluoride Solid-Electrolyte Materials via Screening the Structural Property of Li-Ion Sublattice, Nano Energy 79 (2021), 105407.
[10] C.V. Chandran, P. Heitjans, Solid-State NMR Studies of Lithium Ion Dynamics Across Materials Classes, Ann. Rep. NMR Spectrosc. 89 (2016) 1–102.
[11] C.V. Chandran, P. Heitjans, Solid-State NMR Studies of Lithium Ion Dynamics Across Materials Classes: Review Update, Ann. Rep. NMR Spectrosc. 106 (2022) 1–51.
[12] Y.J. Lee, F. Wang, C.P. Grey, ^{6}Li and ^{7}Li MAS NMR Studies of Lithium Manganate Cathode Materials, J. Am. Chem. Soc. 120 (1998) 12601–12613.
[13] C. Pan, Y.J. Lee, B. Ammundsen, C.P. Grey, ^{6}Li MAS NMR Studies of the Local Structure and Electrochemical Properties of Cr-doped Lithium Manganese and Lithium Cobalt Oxide Cathode Materials for Lithium-Ion Batteries, Chem. Mater. 14 (2002) 2289–2299.
[14] C.P. Grey, N. Dupré, NMR Studies of Cathode Materials for Lithium-Ion Rechargeable Batteries, Chem. Rev. 104 (2004) 4493–4512.
[15] J. Wontcheu, W. Bensch, M. Wilkening, P. Heitjans, S. Indris, P. Sideris, C.P. Grey, S. Mankovsky, H. Ebert, Tuning the Structural and Physical Properties of $Cr_2Ti_3Se_8$ by Lithium Intercalation: A study of the Magnetic Properties, Investigation of Ion Mobility with NMR Spectroscopy and Electronic Band structure Calculations, J. Am. Chem. Soc. 130 (2008) 288–299.
[16] O. Pecher, J. Carretero-Gonzalez, K.J. Griffith, C.P. Grey, Materials' Methods: NMR in Battery Research, Chem. Mater. 29 (2017) 213–242.
[17] S. Britto, I.D. Seymour, D. Halat, M.F.V. Hidalgo, C. Siu, P.J. Reeves, H. Zhou, N. A. Chernova, M.S. Whittingham, C.P. Grey, Evolution of Lithium Ordering with (De)-Lithiation in b-$LiVOPO_4$: Insights through Solid-State NMR and First Principles DFT Calculations, J. Mater. Chem. A 8 (2020) 5546–5557.
[18] D. Carlier, M. Ménétrier, C. Delmas, Transferred Hyperfine Interaction between a Tetrahedral Transition Metal and Tetrahedral Lithium: Li_6CoO_4, J. Phys. Chem. C 114 (2010) 4749–4755.
[19] C. Chazel, M. Ménétrier, L. Croguennec, C. Delmas, $^{6/7}$Li NMR Study of the $Li_{1-z}Ni_{1+z}O_2$ phases, Magn. Reson. Chem. 43 (2005) 849–857.
[20] D. Carlier, M. Ménétrier, C.P. Grey, C. Delmas, G. Ceder, Understanding the NMR Shifts in Paramagnetic Transition Metal Oxides Using Density Functional Theory Calculations, Phys. Rev. B 67 (2003), 174103.

[21] L.S. Cahill, R.P. Chapman, C.W. Kirby, G.R. Goward, The Challenge of Paramagnetism in Two-Dimensional ^{6,7}Li Exchange NMR, Appl. Magn. Reson. 32 (2007) 565–581.
[22] J. Langer, D.L. Smiley, A.D. Bain, G.R. Goward, M. Wilkening, An Unexpected Pathway: ^{6}Li-Exchange NMR Spectroscopy Points to Vacancy-Driven Out-of-Plane Li-Ion Hopping in Crystalline Li_2SnO_3, J. Phys. Chem. C 120 (2016) 3130–3138.
[23] E. Witt, C.V. Chandran, P. Heitjans, Slow Ion Exchange in Crystalline $Li_2SO_4 \cdot H_2O$: A ^{6}Li 2D EXSY NMR Investigation, Solid State Ionics 304 (2017) 60–64.
[24] M. Wilkening, E.E. Romanova, S. Nakhal, D. Weber, M. Lerch, P. Heitjans, Time-Resolved and Site-Specific Insights into Migration Pathways of Li^+ in a-Li_3VF_6 by Li-6 2D Exchange MAS NMR, J. Phys. Chem. C 114 (2010) 19083–19088.
[25] P. Bottke, D. Freude, M. Wilkening, Ultraslow Li Exchange Processes in Diamagnetic Li_2ZrO_3 As Monitored by EXSY NMR, J. Phys. Chem. C 117 (2013) 8114–8119.
[26] L.S. Cahill, R.P. Chapman, J.F. Britten, G.R. Goward, ^{7}Li NMR and Two-Dimensional Exchange Study of Lithium Dynamics in Monoclinic $Li_3V_2(PO_4)_3$, J. Phys. Chem. B 110 (2006) 7171–7177.
[27] L.J.M. Davis, B.L. Ellis, T.N. Ramesh, L.F. Nazar, A.D. Bain, G.R. Goward, ^{6}Li 1D EXSY NMR Spectroscopy: A New Tool for Studying Lithium Dynamics in Paramagnetic Materials Applied to Monoclinic Li_2VPO_4F, J. Phys. Chem. C 115 (2011) 22603–22608.
[28] Y. Makimura, L.S. Cahill, Y. Iriyama, G.R. Goward, L.F. Nazar, Layered Lithium Vanadium Fluorophosphate, $Li_5V(PO_4)_2F_2$: A 4 V Class Positive Electrode Material for Lithium-Ion Batteries, Chem. Mater. 20 (2008) 4240–4248.
[29] Z. Xu, J.F. Stebbins, Cation Dynamics and Diffusion in Lithium Orthosilicate: Two-Dimensional ^{6}Li NMR, Science 270 (1995) 1332–1334.
[30] V.W.J. Verhoeven, I.M. de Schepper, G. Nachtegaal, A.P.M. Kentgens, E.M. Kelder, J. Schoonman, F.M. Mulder, Lithium Dynamics in $LiMn_2O_4$ Probed Directly by Two-Dimensional ^{7}Li NMR, Phys. Rev. Lett. 86 (2001) 4314–4317.
[31] L.J.M. Davis, I. Heinmaa, G.R. Goward, Study of Lithium Dynamics in Monoclinic $Li_3Fe_2(PO4)_3$ using ^{6}Li VT and 2D Exchange MAS NMR Spectroscopy, Chem. Mater. 22 (2010) 769–775.
[32] R.J. Messinger, M. Ménétrier, E. Salager, A. Boulineau, M. Duttine, D. Carlier, J.-M. Ateba Mba, L. Croguennec, C. Masquelier, D. Massiot, M. Deschamps, Revealing Defects in Crystalline Lithium-Ion Battery Electrodes by Solid-State NMR: Applications to $LiVPO_4F$, Chem. Mater. 27 (2015) 5212–5221.
[33] V.K. Michaelis, K. Levin, Y. Germanov, G. Lelong, S. Kroeker, Ultrahigh-Resolution ^{7}Li Magic-Angle Spinning Nuclear Magnetic Resonance Spectroscopy by Isotopic Dilution, Chem. Mater. 30 (2018) 5521–5526.
[34] J. Kohl, D. Wiedemann, S. Nakhal, P. Bottke, N. Ferro, T. Bredow, E. Kemnitz, M. Wilkening, P. Heitjans, M. Lerch, Synthesis of Ternary Transition Metal Fluorides Li_3MF_6 via a Sol-Gel Route as Candidates for Cathode Materials in Lithium-Ion Batteries, J. Mater. Chem. 22 (2012) 25496. -25496.
[35] E. Fukushima, S.B.W. Roeder, Experimental Pulse NMR, Addison-Wesley, 1981. Reading.
[36] L. Peng, R.J. Clément, M. Lin, Y. Yang, NMR and MRI of Electrochemical Energy Storage Materials and Devices, The Royal Society of Chemistry, 2021, pp. 1–70.
[37] D. Suter, R.R. Ernst, Spin Diffusion in Resolved Solid-State NMR Spectra, Phys. Rev. B 32 (1985) 5608–5627.
[38] L.L. Wong, K.C. Phuah, R. Dai, H. Chen, W.S. Chew, S. Adams, Bond Valence Pathway Analyzer - An Automatic Rapid Screening Tool for Fast Ion Conductors within softBV, Chem. Mater. 33 (2021) 625–641.
[39] H. Chen, L.L. Wong, S. Adams, SoftBV - A Software Tool for Screening the Materials Genome of Inorganic Fast Ion Conductors, Acta Cryst. B Struct. Sci. Cryst. Eng. Mater. 75 (2019) 18–33.
[40] C. Müller, E. Zienicke, S. Adams, J. Habasaki, P. Maass, Comparison of Ion Sites and Diffusion Paths in Glasses Obtained by Molecular Dynamics Simulations and Bond Valence Analysis, Phys. Rev. B 75 (2007).
[41] M.M. Islam, M. Wilkening, P. Heitjans, T. Bredow, Insights into Li^+ Migration Pathways in α-Li_3VF_6: A First-Principles Investigation, J. Phys. Chem. Lett. 3 (2012) 3120–3124.